46th AIAA Aerospace Sciences Meeting and Exhibit
7 - 10 January 2008, Reno, Nevada

AIAA 2008-1048

Comparison of Subfilter Scale Models for LES of Turbulent Premixed Flames

W. Lin*, F. E. Hernández-Pérez†, C. P. T. Groth‡ and Ö. L. Gülder§
University of Toronto Institute for Aerospace Studies
Toronto, Ontario, M3H 5T6, Canada

The role of subfilter scale models for representing turbulence-chemistry interactions in large eddy simulations (LES) of turbulent premixed combustion is of considerable importance as the internal structure of premixed flames is generally smaller than the filter sizes. Moreover, the accuracy and validity of LES subfilter scale models for premixed combustion are still under debate. A detailed comparison is made between two laminar flamelet type modeling approaches: one approach based on the thickened flame and power-law flame wrinkling models and a second approach based on the flame surface density (FSD) model. The strengths and limitations of both methods are examined and the numerical predictions of the thickened flame and FSD models are investigated and compared for freely propagating premixed flames. The numerical results also include a discussion of the influence of turbulence intensity on the turbulent flame speed and flame structure. The study is intended to provide insight into the computational and physical modeling requirements for performing LES of turbulent premixed flames.

I. Introduction

The numerical modeling of turbulent reactive flows represents a significant computational challenge as such flows involve a broad range of complex physical and chemical phenomena occurring over a wide range of spatial and temporal scales. Large Eddy Simulation (LES) is proving to be a valuable tool for numerical solution of non-reacting turbulent flows,[1] but it is at an early stage in its application to turbulent combusting flows. One of the main challenges of LES for premixed turbulent combustion is that, in many cases, the internal flame structure is entirely on the subfilter scales and, because of this, the accuracy and validity of LES subfilter scale models for representing the effects of scales generally smaller than the filter size are still under debate.[2]

In premixed flames, the reactants (fuel and oxidizer mixed at the molecular level) and burnt gases (combustion products) are separated by a thin reaction zone or surface having a characteristic propagation speed (flame speed) and thickness. Models for premixed turbulent combustion are therefore often geometrical in nature with mixture properties (mass fractions, chemical kinetics, etc.) related to the dynamics and properties of iso-surfaces. This study considers a comparison of two different modeling approaches for turbulent premixed flames: one approach based on the thickened flame and power-law flame wrinkling models[3,4] and a second approach based on a flame surface density (FSD) transport equation.[5,6] Both of these approaches are laminar flamelet type models.[7] The thickened flame and FSD models are compared and LES results obtained using both approaches for prediction of freely propagating premixed flames are described. Results for stoichiometric flames are considered. A parallel adaptive mesh refinement algorithm has been developed and is used herein for the solution of the Favre-filtered Navier-Stokes equations for a compressible reactive thermally perfect mixture.[8,9] The numerical results include a discussion of the influence of turbulence intensity on the turbulent flame speed and flame structure. In what follows is a discussion of the subfilter-scale

*PhD Candidate, wlin@utias.utoronto.ca
†PhD Candidate, hperez@utias.utoronto.ca
‡Associate Professor, Senior Member AIAA, groth@utias.utoronto.ca
§Professor, Senior Member AIAA, ogulder@utias.utoronto.ca

modeling, numerical solution scheme, and preliminary computational results for freely propagating flames in both two-dimensional and three-dimensional decaying isotropic homogeneous turbulent fields.

II. Favre-Filtered Governing Equations

In LES, a separation of scales is achieved via a low-pass filtering procedure. Scales larger than the filter size, Δ, are resolved, whereas scales smaller than Δ are modeled. Relevant flow quantities, ϕ, are filtered or Favre-filtered (mass-weighted filtering) to give $\overline{\phi}$ or $\widetilde{\phi}$, respectively. The Favre-filtered form of the Navier-Stokes equations governing compressible flows of a thermally perfect reactive mixture of gases are used herein to describe turbulent premixed combustion processes. They are given by

$$\frac{\partial}{\partial t}\left(\bar{\rho}\right) + \frac{\partial}{\partial x_i}\left(\bar{\rho}\tilde{u}_i\right) = 0\,, \tag{1}$$

$$\frac{\partial}{\partial t}\left(\bar{\rho}\tilde{u}_i\right) + \frac{\partial}{\partial x_j}\left(\bar{\rho}\tilde{u}_i\tilde{u}_j + \delta_{ij}\bar{p} - \check{\tau}_{ij}\right) = A_1 + A_2\,, \tag{2}$$

$$\frac{\partial}{\partial t}\left(\bar{\rho}\tilde{E}\right) + \frac{\partial}{\partial x_i}\left[\left(\bar{\rho}\tilde{E} + \bar{p}\right)\tilde{u}_i + \check{q}_i\right] - \frac{\partial}{\partial x_j}\left(\check{\tau}_{ij}\tilde{u}_i\right) = B_1 + B_2 + B_3 + B_4 + B_5 + B_6\,, \tag{3}$$

$$\frac{\partial}{\partial t}\left(\bar{\rho}\tilde{Y}_k\right) + \frac{\partial}{\partial x_i}\left(\bar{\rho}\tilde{Y}_k\tilde{u}_i\right) + \frac{\partial \check{\mathcal{J}}_{k,i}}{\partial x_i} = \overline{\dot{\omega}}_k + C_1 + C_2\,, \tag{4}$$

where $\bar{\rho}$ is the filtered mixture density, $\tilde{u}_i$ is the Favre-filtered mixture velocity, $\bar{p}$ is the filtered mixture pressure, $\tilde{Y}_k$ is the Favre-filtered mass fraction of species k, $\tilde{E}$ is the Favre-filtered total mixture energy (including chemical energy) given by $\tilde{E} = \sum_{k=1}^{N}\tilde{Y}_k(\check{h}_k + \Delta h^0_{f,k}) - \bar{p}/\bar{\rho} + \widetilde{u_i u_i}/2$, $\check{h}_k$ and $\Delta h^0_{f,k}$ are the sensible enthalpy and heat of formation for species k, respectively, and $\overline{\dot{\omega}}_k$ is the filtered reaction rate. The filtered equation of state has the form $\bar{p} = \bar{\rho}R\tilde{T} + D_1$. The resolved viscous stress tensor, $\check{\tau}_{ij}$, the resolved total heat flux, $\check{q}_i$, and the resolved species diffusive fluxes, $\check{\mathcal{J}}_{k,i}$, are evaluated in terms of the filtered quantities as: $\check{\tau}_{ij} = 2\check{\mu}(\check{S}_{ij} - \delta_{ij}\check{S}_{ll}/3)$, $\check{q}_i = -\check{\kappa}\partial\tilde{T}/\partial x_i + \sum_{k=1}^{N}\check{h}_k\check{\mathcal{J}}_{k,i}$, $\check{\mathcal{J}}_{k,i} = -\bar{\rho}\check{D}_k\partial\tilde{Y}_k/\partial x_i$, where $\tilde{T}$ is the mixture temperature, $\check{\mu}$ is the mixture viscosity, $\check{\kappa}$ is the mixture thermal conductivity, and $\check{D}_k$ is the diffusivity of species k with respect to the mixture, and the strain rate tensor, $\check{S}_{ij}$, is given by $\check{S}_{ij} = (\partial\tilde{u}_i/\partial x_j + \partial\tilde{u}_j/\partial x_i)/2$.

The terms, A_1, A_2, B_1, B_2, B_3, B_4, B_5, B_6, C_1, C_2, and D_1, arise from the low-pass filtering process and require modeling. In most LES, the terms A_2, B_2, B_3, B_5, C_2, and D_1 are assumed to be small and are neglected.[10] The non-negligible terms are

$$A_1 = -\frac{\partial}{\partial x_j}\left[\bar{\rho}\left(\widetilde{u_i u_j} - \tilde{u}_i\tilde{u}_j\right)\right]\,, \qquad B_1 = -\frac{\partial}{\partial x_i}\left[\bar{\rho}\left(\widetilde{hu_i} - \tilde{h}\tilde{u}_i\right)\right]\,,$$

$$B_4 = -\frac{1}{2}\frac{\partial}{\partial x_i}\left[\bar{\rho}\left(u_j\widetilde{u_j u_i} - \tilde{u}_j\tilde{u}_j\tilde{u}_i\right)\right]\,, \qquad C_1 = -\frac{\partial}{\partial x_i}\left[\bar{\rho}\left(\widetilde{Y_k u_i} - \tilde{Y}_k\tilde{u}_i\right)\right]\,,$$

(B_6 is related to C_1) and must be modeled for closure of the filtered equation set. In LES, the subfilter stresses, $\sigma_{ij} = -\bar{\rho}(\widetilde{u_i u_j} - \tilde{u}_i\tilde{u}_j)$, are generally modeled using an eddy-viscosity model with $\sigma_{ij} = 2\bar{\rho}\nu_t(\check{S}_{ij} - \delta_{ij}\check{S}_{ll}/3) + \delta_{ij}\sigma_{ll}/3$. The eddy viscosity, ν_t, is prescribed herein by using either the standard Smagorinsky model[11] or a one-equation model.[5] In the Smagorinsky model, $\nu_t = C_s\Delta^2|\tilde{S}|$, the trace, σ_{ll}, is specified using the Yoshizawa model[12] with $\sigma_{ll} = -2\bar{\rho}C_I\Delta^2|\check{S}|^2$, and C_s and C_I are model constants that must be specified. In the one-equation model, $\nu_t = C_\nu\Delta\tilde{k}^{1/2}$, where C_ν is a model constant, $\sigma_{ll} = -2\bar{\rho}\tilde{k}$, and $\tilde{k}$ is the subfilter turbulent kinetic energy. A modeled transport equation is solved for $\tilde{k}$.

Standard gradient-based approximations are used in this work for the modeling of the subfilter-scale fluxes B_1, B_6, and C_1: $\bar{\rho}(\widetilde{hu_i} - \tilde{h}\tilde{u}_i) = -(\check{C}_p\bar{\rho}\nu_t/\mathrm{Pr}_t)\partial\tilde{T}/\partial x_i$ and $\bar{\rho}(\widetilde{u_i Y_k} - \tilde{u}_i\tilde{Y}_k) = -(\bar{\rho}\nu_t/\mathrm{Sc}_t)\partial\tilde{Y}_k/\partial x_i$, where Pr_t and Sc_t are subfilter-scale turbulent Prandtl and Schmidt numbers. The subfilter turbulent diffusion term, B_4, is modeled as suggested by Knight *et al.*[13] with $-\bar{\rho}(u_i\widetilde{u_i u_j} - \tilde{u}_i\tilde{u}_i\tilde{u}_j)/2 = \sigma_{ij}\tilde{u}_i$.

III. Thickened Flame Model

III.A. Artificially Thickened Flame

The challenge in LES for reactive flows is to accurately model the influence of the subfilter-scale turbulence on the filtered reaction rates, $\overline{\dot{\omega}}_k$. This is particularly challenging for turbulent premixed combustion where the flame thickness, δ, is 0.1–1.0 mm, and this is in many cases smaller than practical LES filter widths, Δ. One approach to modeling the turbulence/chemistry interaction for premixed flames is offered by the so-called thickened flame model. In the thickened flame model, the computed flame front structure is artificially locally thickened in such a way that it can be resolved on a coarse LES mesh, but such that the laminar flame speed remains unaltered.[14] From the theory of laminar premixed flames, it is well established that the laminar flame speed, $s_{\rm L}$, and the laminar flame thickness, $\delta_{\rm L}$, scale as $s_{\rm L} \propto \sqrt{D\dot{\omega}}$ and $\delta_{\rm L} \propto D/s_{\rm L}$, where D is the molecular diffusivity and $\dot{\omega}$ the reaction rate. Thus, an increase in flame thickness by a factor F with a constant flame speed, can be achieved by multiplying the molecular diffusivity D by F, and the reaction rate $\dot{\omega}$ by $1/F$. An efficiency factor, $E_{\rm F}$, is also introduced to account for the resulting decrease in the Damkhöler number, Da, for the flame.[3] The resulting filtered balance equation for chemical species takes the modified form

$$\frac{\partial}{\partial t}\left(\bar{\rho}\tilde{Y}_k\right) + \frac{\partial}{\partial x_i}\left(\bar{\rho}\tilde{Y}_k\tilde{u}_i\right) = \frac{\partial}{\partial x_i}\left[E_{\rm F}F\bar{\rho}\left(\check{D}_k + \frac{\nu_t}{{\rm Sc}_t}\right)\frac{\partial \tilde{Y}_k}{\partial x_i}\right] + \frac{E_{\rm F}\overline{\dot{\omega}}_k}{F}\,, \tag{5}$$

where the filtered reaction rates, $\overline{\dot{\omega}}_k$, are now calculated directly using Arrhenius law reaction rates evaluated in terms of resolved quantities.

Besides allowing the representation of the flame front on relatively coarse grids, the thickened flame approach allows one to take into account phenomena such as ignition, flame stabilization and flame-wall interaction because of the direct use of Arrhenius-law chemical kinetics. Also, if molecular diffusion is described by Fick's law, this approach can potentially be extended to complex chemistry.

III.B. Power-Law Flame Wrinkling Model

To correct the flame Damkhöler number and incorporate the influences of the unresolved turbulent field on the chemical kinetics, the efficiency factor, $E_{\rm F}$, is evaluated herein using a power-law flame wrinkling model. Assuming that the internal structure of the flame is not significantly altered by the turbulence, as in the wrinkled flamelets, corrugated flamelets, and thin reaction zones premixed combustion regimes,[7] and that the increased flame surface area due to the flame front wrinkling by the subfilter-scale turbulence leads to an increase in the flame speed, a power-law expression is used to evaluate $E_{\rm F}$ given by[4,15]

$$\frac{s_{{\rm T}\Delta_{\rm o}}}{s_{\rm L}} = \frac{A_{\Delta_{\rm o}}}{\Delta^2} = \Xi_{\Delta_{\rm o}} = \left(1 + \frac{\Delta_{\rm o}}{\eta_{\rm i}}\right)^{\gamma} = E_{\rm F}\,, \tag{6}$$

where $s_{{\rm T}\Delta_{\rm o}}$ is the subfilter turbulent flame speed, $\Xi_{\Delta_{\rm o}}$ is the subfilter wrinkling factor, $\Delta_{\rm o}$ is the outer cutoff scale, $\eta_{\rm i}$ is the inner cutoff scale, and γ is the power of the expression, which is taken to be 0.5 here.[4] The inner cutoff is associated with the maximum of the laminar flame thickness and the mean curvature of the flame, which can be estimated by assuming an equilibrium between production and destruction of flame surface density as $\mid \langle \nabla \cdot \mathbf{n} \rangle_{\rm s} \mid = \Delta_{\rm o}^{-1}(u'_{\Delta_{\rm o}}/s_{\rm L})\Gamma_{\Delta_{\rm o}}(\Delta_{\rm o}/\delta_{\rm L}, u'_{\Delta_{\rm o}}/s_{\rm L}, Re_{\Delta_{\rm o}})$, where $\Gamma_{\Delta_{\rm o}}$ is the efficiency function proposed by Charlette *et al.*[4] to account for the net straining of all relevant scales smaller than $\Delta_{\rm o}$. The subfilter Reynolds number, $Re_{\Delta_{\rm o}}$, is based on the subfilter-scale rms velocity $u'_{\Delta_{\rm o}}$, calculated using the expression proposed by Colin *et al.*,[3] $u'_{\Delta_{\rm o}} = c_2\Delta_x^3 \mid \nabla^2(\nabla \times \tilde{\mathbf{u}}) \mid$. The model constant c_2 is set to 1.545 in this work for the two-dimensional simulations.[3] The wrinkling factor can then be rewritten as

$$\Xi_{\Delta_{\rm o}} = \left(1 + \min\left[\frac{\Delta_{\rm o}}{\delta_{\rm L}}\,,\, \Gamma_{\Delta_{\rm o}}\frac{u'_{\Delta_{\rm o}}}{s_{\rm L}}\right]\right)^{\gamma} = E_{\rm F}\,. \tag{7}$$

IV. Flame Surface Density Model

IV.A. Transport of Progress Variable

In the LES context, a second approach to modeling of turbulent premixed flames is to ignore for the most part its internal structure and detailed chemical kinetics and represent the combustion occurring at the thin flame front in terms of a reaction progress variable that quantifies the conversion of reactants to products. One possible definition of a progress variable, c, is provided by a reduced fuel mass fraction, $c = (Y_F - Y_F^u)/(Y_F^b - Y_F^u)$, where Y_F, Y_F^u and Y_F^b are respectively the local, unburnt and burnt fuel mass fractions.[10] The progress variable takes on values in the range $0 \leq c \leq 1$ with $c = 0$ in the fresh gases and $c = 1$ in the fully burnt gases. The composition of the reactive mixture, in terms of the mass fractions of the reactants and products, can then be specified directly in terms of the progress variable. A Favre-filtered progress variable transport equation can be derived having the form

$$\frac{\partial}{\partial t}\left(\bar{\rho}\tilde{c}\right) + \frac{\partial}{\partial x_i}\left(\bar{\rho}\tilde{c}\tilde{u}_i\right) = \overline{\frac{\partial}{\partial x_i}\left(\rho D \frac{\partial c}{\partial x_i}\right)} + \overline{\dot{\omega}} - \frac{\partial}{\partial x_i}\left[\bar{\rho}\left(\widetilde{cu_i} - \tilde{c}\tilde{u}_i\right)\right], \tag{8}$$

where the unclosed diffusive flux, $\overline{\nabla(\rho D \nabla c)}$, and filtered reaction rate, $\overline{\dot{\omega}}$, are modeled together as

$$\begin{aligned}\overline{\dot{\omega}} + \overline{\nabla(\rho D \nabla c)} = \overline{\rho w |\nabla c|} &= \int_0^1 \overline{(\rho w)}_{\mathrm{s}} \bar{\rho}\tilde{\Sigma} dc^* \\ &\approx \overline{(\rho w)}_{\mathrm{s}} \bar{\rho}\tilde{\Sigma} \approx \rho_r s_{\mathrm{L}} \bar{\rho}\tilde{\Sigma},\end{aligned} \tag{9}$$

and a gradient transport model is adopted for $\bar{\rho}(\widetilde{cu_i} - \tilde{c}\tilde{u}_i) = -(\bar{\rho}\nu_t/\mathrm{Sc}_t)\partial\tilde{c}/\partial x_i$.[5] The resulting modeled progress variable equation is given by

$$\frac{\partial}{\partial t}\left(\bar{\rho}\tilde{c}\right) + \frac{\partial}{\partial x_i}\left(\bar{\rho}\tilde{c}\tilde{u}_i\right) = \frac{\partial}{\partial x_i}\left(\frac{\bar{\rho}\nu_t}{\mathrm{Sc}_t}\frac{\partial \tilde{c}}{\partial x_i}\right) + \rho_r s_{\mathrm{L}} \bar{\rho}\tilde{\Sigma}, \tag{10}$$

where ρ_r is the reactants density, $\tilde{\Sigma}$ is the Favre-filtered flame surface area per unit mass of the mixture, and the product, $\bar{\rho}\tilde{\Sigma}$, is the flame surface area per unit volume or flame surface density (FSD). A means for specifying the FSD is required to provide closure for this description of premixed flames.

IV.B. Transport of Flame Surface Density

The filtered quantity, $\tilde{\Sigma}$, includes contributions from the resolved FSD and the unresolved subfilter-scales. The latter must be modeled. Mathematically, the FSD can be defined as $\bar{\rho}\tilde{\Sigma} = \overline{|\nabla c|\delta(c^* - c)}$. A modeled transport equation for the flame surface density has been proposed by Hawkes and Cant[5,6] given by:

$$\begin{aligned}\frac{\partial}{\partial t}\left(\bar{\rho}\tilde{\Sigma}\right) + \frac{\partial}{\partial x_i}\left(\bar{\rho}\tilde{u}_i\tilde{\Sigma}\right) - \frac{\partial}{\partial x_i}\left(\frac{\bar{\rho}\nu_t}{\mathrm{Sc}_t}\frac{\partial \tilde{\Sigma}}{\partial x_i}\right) &= (\delta_{ij} - n_{ij})\bar{\rho}\tilde{\Sigma}\frac{\partial \tilde{u}_i}{\partial x_j} - \frac{\partial}{\partial x_i}[s_{\mathrm{L}}(1+\tau\tilde{c})M_i\bar{\rho}\tilde{\Sigma}] \\ &\quad + s_{\mathrm{L}}(1+\tau\tilde{c})\bar{\rho}\tilde{\Sigma}\frac{\partial M_i}{\partial x_i} + \Gamma_K \bar{\rho}\tilde{\Sigma}\frac{\sqrt{\tilde{k}}}{\Delta} - \beta s_{\mathrm{L}}\frac{(\bar{\rho}\tilde{\Sigma})^2}{1-\tilde{c}},\end{aligned} \tag{11}$$

where $\vec{M} = -\nabla\bar{c}/\tilde{\Sigma}$ is the flamelet model for the surface averaged normal ($\bar{c}$ is estimated using $\bar{c} = (1+\tau)\tilde{c}/(1+\tau\tilde{c})$), $\alpha = 1 - \vec{M}\cdot\vec{M}$, and $n_{ij} = M_i M_j + 1/3\alpha\delta_{ij}$. The variable $\tau = (T_{ad} - T_r)/T_r$ is the heat release parameter, where T_{ad} and T_r are the adiabatic and the reactants temperature, respectively, β is a model constant and must satisfy $\beta \geq 1$ for realisability requirements,[5] α is a resolution factor, and Γ_K is an efficiency function.[16] The terms on the right hand side of the modeled FSD equation represent the production/destruction sources associated with resolved strain, resolved propagation and curvature, and subfilter-scale strain and curvature.

V. Numerical Solution Scheme

A second-order accurate parallel finite-volume scheme has been developed and used to solve the Favre-filtered transport equations described above on multi-block quadrilateral (two space dimensions) and hexahedral

(three space dimensions) computational meshes.[8,9,17] The inviscid flux at each cell face is evaluated using limited linear reconstruction[18] and Riemann-solver or flux-vector-splitting based flux functions,[19,20] while the viscous flux is evaluated utilizing a centrally-weighted diamond-path reconstruction method.[21] A low-Mach number preconditioned dual time-stepping method[22] is used to solve the coupled set of non-linear ordinary differential equations that arise from the spatial discretization procedure. Parallel implementation of the finite-volume scheme has been carried out via domain decomposition using the C++ programming language and the MPI (message passing interface) library.[23]

In two space dimensions, a block-based adaptive mesh refinement (AMR) approach has also been developed for use in conjunction with the finite-volume method described above. A flexible block-based hierarchical data structure has been devised and is used to facilitate automatic solution-directed mesh adaptation on the multi-block body-fitted mesh according to physics-based refinement criteria. The method allows for anisotropic mesh refinement and is well suited to the domain decomposition procedure used in the parallel implementation. Refer to the recent papers by Sachdev *et al.*[24] and Northrup and Groth[8] for further details. The extension of this approach to three space dimensions is the subject of current research and is on-going.[17]

V.A. Thermodynamic and Transport Properties

For the numerical results presented herein, thermodynamic and molecular transport properties of each mixture component are prescribed using the database compiled by Gordon and McBride,[25,26] which provides curve fits for the species enthalpy, specific heat, viscosity, and thermal conductivity, as functions of temperature. The mixture rules of Wilke[27] and Mason and Saxena[28] are used to determine the molecular viscosity and thermal conductivity of the reactive mixture, respectively.

In our implementation of the thickened flame model, the thickening is applied only on the flame front. The heat conductivity, $\check{\kappa}$, the molecular diffusivities, $\check{D}_k$, and the molecular viscosity, $\check{\mu}$, are all multiplied by the thickening factor, F, and the efficiency factor, E_{F}. In this way, the Lewis number, Le, Prandtl number, Pr, and Schmidt number, Sc, remain unaffected by the thickening of the flame.

V.B. Reduced Chemical Kinetics

For the FSD model, methane-air chemistry is represented simply by a one-step mechanism and the species mass fractions are formulated as algebraic functions of the progress variable, $\tilde{c}$, such that $\tilde{Y}_k = \tilde{Y}_k(\tilde{c})$. The one-step reaction mechanism for methane combustion is

$$\mathrm{CH_4} + 2\ \mathrm{O_2} \rightarrow \mathrm{CO_2} + 2\ \mathrm{H_2O}\,. \tag{12}$$

For the thickened flame simulations, the chemical kinetics for oxidation of methane is represented by a reduced two-step reaction mechanism, as described by Westbrook and Dryer.[29] In this mechanism, the oxidation of methane is expressed as follows:

$$2\ \mathrm{CH_4} + 3\ \mathrm{O_2} \rightleftharpoons 2\ \mathrm{CO} + 4\ \mathrm{H_2O}\,, \tag{13}$$

$$2\ \mathrm{CO} + \mathrm{O_2} \rightleftharpoons 2\ \mathrm{CO_2}\,. \tag{14}$$

VI. Results for Two-Dimensional Freely Propagating Flames

In order to carry out the comparison of the predictive capabilities of the thickened flame and flame surface density models, freely propagating stoichiometric premixed methane-air flames were first studied in decaying two-dimensional isotropic turbulent fields. Although it can be argued that two-dimensional turbulence differs from three-dimensional turbulence by the absence of the vortex stretching mechanism, turbulent curvature statistics suggest that the three-dimensional topology of a propagating surface is primarily two-dimensional.[30,31] Moreover, the two-dimensional premixed flame studies provided a solid basis for performing the subsequent three-dimensional simulations and evaluating and interpreting the results.

The two-dimensional stoichiometric turbulent flames are initialized by introducing a one-dimensional planar laminar premixed flame on to the computational domain with an isotropic turbulent field superimposed.

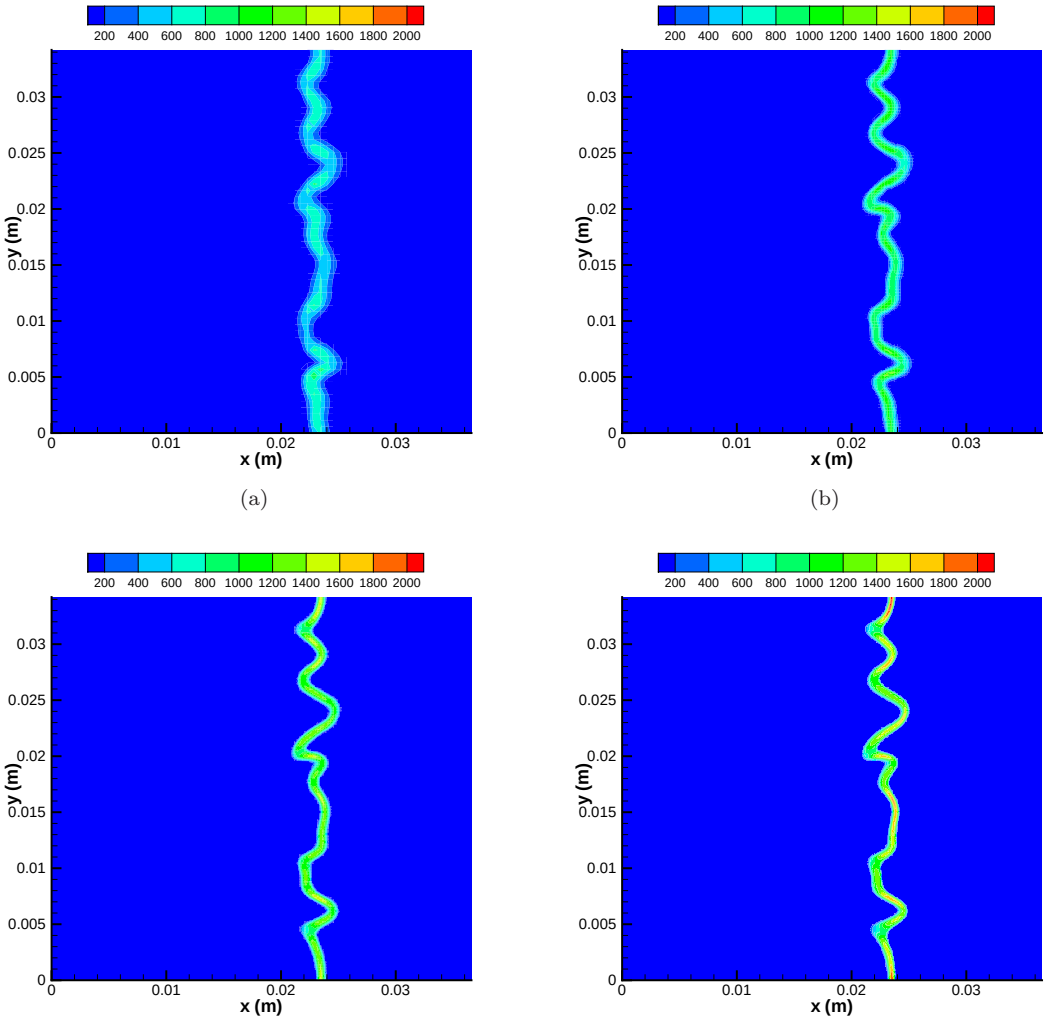

Figure 1. Predicted contours of the flame surface density, $\bar{\rho}\tilde{\Sigma}$, at $t = 0.3$ ms. Results are shown for four different computational grids: (a) uniform mesh with 64×64 cells; (b) uniform mesh with 128×128 cells; (c) uniform mesh with 256×256 cells; and (d) uniform mesh with 512×512 cells.

Subsonic boundary conditions are prescribed at inflow and outflow boundaries, and periodic boundary conditions are applied at the top and bottom of the domain. The turbulent flow field is generated by prescribing a specified synthetic energy spectrum[32] and using the procedure developed by Rogallo.[33]

The turbulent burning rates for these cases are computed, based on the integrated consumption rate of fuel and the integrated FSD, in the thickened flame and FSD simulations, respectively. The corresponding expressions for the thickened flame and FSD burning rates are given by

$$s_{\mathrm{T}} = \frac{1}{\bar{\rho}_r \tilde{Y}_{F_r} L_y} \int_A \overline{\dot{\omega}}_F dA\,, \tag{15}$$

and

$$s_{\mathrm{T}} = \frac{s_{\mathrm{L}}}{L_y} \int_A \bar{\rho}\tilde{\Sigma} dA\,, \tag{16}$$

where $\bar{\rho}_r$ is the reactants density and $\tilde{Y}_{F_r}$ is the fuel mass fraction in the reactants.

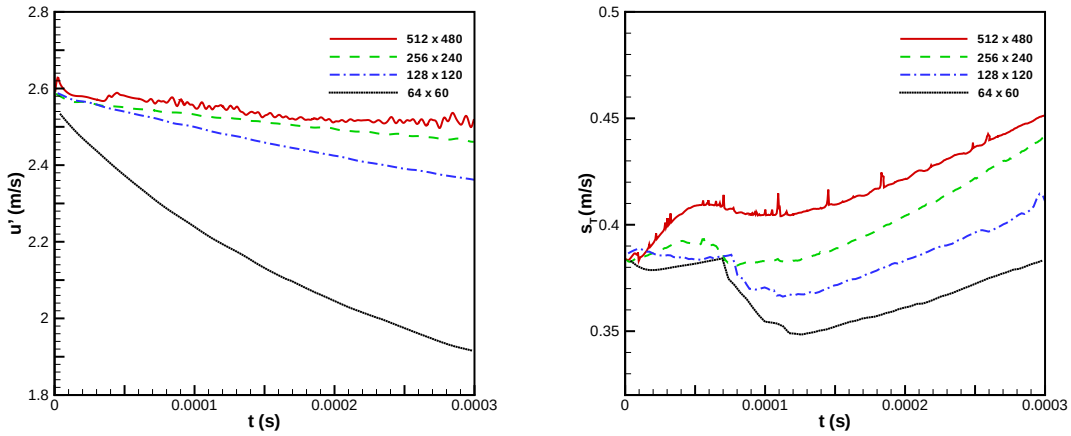

(a) (b)

Figure 2. Predicted decay of resolved turbulence intensity (a) and predicted turbulent burning rate (b) for the different mesh resolutions: uniform mesh with 64×64 cells; uniform mesh with 128×128 cells; uniform mesh with 256×256 cells; and uniform mesh with 512×512 cells.

VI.A. Influence of Mesh Resolution

Before comparing the two subfilter scale models in detail, it was felt that the baseline mesh resolution requirements of the proposed finite-volume scheme for accurately representing the turbulent flow field of interest should be established. Therefore, a study of the influence of the mesh resolution on the solution quality was first carried out. For this purpose, a premixed flame was considered propagating through a homogeneous turbulent field characterized as follows: turbulence intensity, $u' = 2.59$ m/s; integral length scale, $L_{11} = 6.47$ mm; Taylor micro scale, $\lambda = 0.832$ mm; Kolmogorov scale $\eta = 0.06$ mm; turbulent Reynolds number, $Re_\lambda = 137$; laminar flame speed $s_L = 0.38$ m/s; and flame thickness, $\delta_L = 0.44$ mm. The size of the rectangular-shaped domain considered for the simulation is 0.0366 m by 0.0342 m. Four different uniform grids were considered: $64\times60 = 3,840$, $128\times120 = 15,360$, $256\times240 = 61,440$, and $512\times480 = 245,760$ cell meshes with computational cells equally distributed on 48 solution blocks. The cell sizes compared to the Taylor micro scales and Kolmogorov scales for different mesh resolutions are $\Delta x = 0.56\lambda = 7.36\eta$ for 64×60 cells, $\Delta x = 0.33\lambda = 4.14\eta$ for 128×120 cells, $\Delta x = 0.17\lambda = 2.3\eta$ for 256×240 cells, and $\Delta x = 0.08\lambda = 1.17\eta$ for 512×480 cells. For each simulation, the filter width, Δ, was fixed and equal to $\Delta = 2\Delta x_{128\times120}$, where $\Delta x_{128\times120} = 0.267 = 1.25\delta_L$ mm is the mesh spacing of the 128×120 grid. The simulation results are computed up to 0.3 ms corresponding to a time of approximately one eddy turnover based on the Taylor micro scale.

The FSD model was used in the mesh convergence study. The predicted FSD solutions on the four different mesh resolutions are shown in Figures 1(a)–1(d). Colour contours of the predicted values of $\bar{\rho}\tilde{\Sigma}$ are given in the figures with peak values of the FSD occurring within the flame. The wrinkling of the initially planar laminar flame by the resolved turbulent field is quite evident in each case. Although not shown, it is found that there is a corresponding increase in the calculated turbulent flame speed as the simulation progresses until a near equilibrium flame speed is achieved of $s_T = 0.95$ m/s ($s_T/s_L \approx 2.5$) at $t = 1.8$ ms. At that point the predicted turbulent intensity has diminished by more than 30%.

Comparing the results of Figures 1(a)–1(d), it is fairly evident that the coarsest mesh (64×60 cells) does not provide adequate resolution of the flame front as compared to the solution on the finest mesh. The finest mesh (512×480 cells) results in a well resolved thin and smooth flame front with a maximum value for the FSD. Nevertheless, the solutions on the other intermediate meshes (256×240 and 128×120 grids) also show a reasonable agreement with the finest mesh solution in terms of overall flame wrinkling and peak values of the FSD.

Turning attention to the predicted turbulent field, the predicted temporal variations of the resolved turbulence intensity, u', determined for each of the four meshes are shown in Figure 2(a). It may be observed that

the predictions of the u' for the 512×480, 256×240 and 128×120 grids are generally in agreement, in fact it appears that a virtually grid-independent result has been achieved on the 256×240 mesh, whereas the 64×60 grid result is clearly under-resolved. However, even though the turbulence field is generally resolved on the finer meshes, if one considers the predicted turbulent flame speed on each mesh as shown in Figure 2(b), it is quite apparent that the flame front and FSD are still not fully resolved. Even further refinement of the mesh is required to obtain a fully grid-independent solution. Note that similar mesh refinement studies have been performed for the thickened flame model and, as expected, the artificial thickening of the flame front reduces the mesh resolution requirements for obtaining grid-independent burning rates (accurate burning rates can be achieved on more moderately refined meshes).

VI.B. Predicted Flame Structure

Simulations for three different levels of turbulence intensity were carried out. The initial ratios of turbulence intensity to laminar flame speed in the unburnt mixture are: $u'/s_{\mathrm{L}} = 6.8,\ 10.4,\ 20.7$. These cases are identified as case A, case B and case C, respectively. Other parameters characterizing the initial conditions in the unburnt gas are: $L_{11} = 6.4$ mm, $\lambda = 0.83$ mm. The dimensions of the domain for the simulations are $L_x = 0.0366$ m and $L_y = 0.0342$ m, and a 128×120 cell uniform computational mesh with 48 solution blocks was employed. Inflow and outflow subsonic boundary conditions are imposed on the left and right boundaries, respectively, whereas the two remaining boundaries are periodic. A constant thickening factor, $F = 5$, was employed with the thickened flame model.

Figures 3(a)–3(f) show the predicted contours of methane mass fraction at a time equal to 0.6 ms. This time corresponds to roughly two, three and six eddy turnovers based on Taylor scale for cases A, B and C, respectively.

Methane mass fraction contours clearly illustrate the strong influence of the turbulence intensity on the predicted flame structure. For both, the thickened flame and FSD models, there is a significant increase in the resolved flame front wrinkling with turbulent intensity. Comparing the two models, the overall agreement between the predicted flames geometries is rather good. The wrinkling generated by large turbulent structures is similar for both models. Differences are largely due to the fact that the flame front of the thickened model has been artificially thickened and a greater proportion of the flame wrinkling is therefore modeled. The differences become more evident when the flame is subject to higher turbulence levels, as displayed in Figures 3(e) and 3(f). In this case, some of the small wrinkled structures that develop at earlier times in the FSD simulation have grown significantly; however, the same structures are not present in the thickened flame simulation.

FSD contours are shown in Figures 4(b), 4(d) and 4(f). As it can be seen, the maximum values of FSD increase with turbulence intensity. Higher turbulence intensities lead to more flame wrinkling, which in turn, produce more flame surface. A point of note is the thickness associated with the FSD contours. There is a thickening of the FSD, which is due to lack of resolution of the FSD. As noted in the previous subsection, a numerical challenge associated with the FSD approach is that the required resolution of FSD is higher as compared to the thickened flame approach. On the other hand, a reduced number of transport equations needs to be solved when a FSD and progress variable formulation is employed, which, from the computational viewpoint, is advantageous. Another advantage of the FSD approach is the separation of complex chemistry from turbulence in which chemistry modeling is simply incorporated through the laminar flame speed and heat release parameter.

Since the thickened flame approach offers the possibility to deal with a more complex chemical and transport description of a premixed flame, results obtained for an intermediate species like CO are discussed next. Figures 4(a), 4(c) and 4(e) show the CO mass fraction contours. For the three different cases, the largest concentrations of CO tend to occur in regions where the flame front is convex towards the reactants. This is in agreement with direct numerical simulation results reported in references.[34,35] These regions generally coincide with zones where the flame undergoes downstream interaction, which have been reported to be the main areas for CO production. In these regions the CO oxidation layer is curtailed. It is interesting to note that despite the fact that only a two-step reaction mechanism is used in the LES of the premixed flames, important features regarding the interaction between turbulence and chemistry have been captured with thickened flame model.

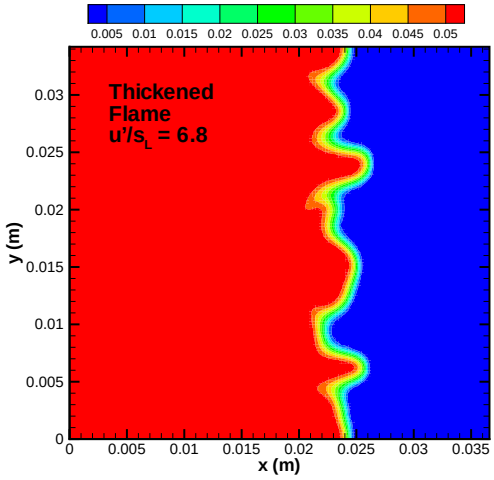

(a) CH_4 mass fraction. Thickened flame, case A, $F = 5$.

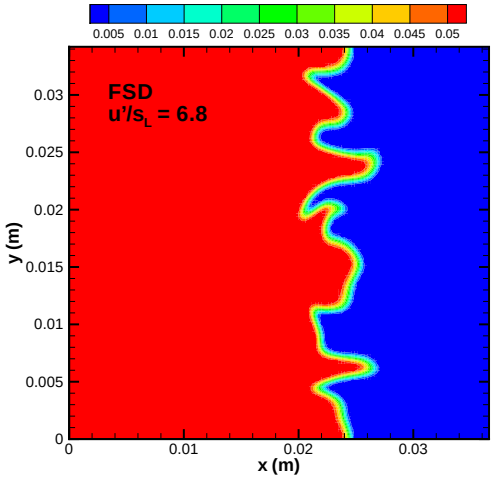

(b) CH_4 mass fraction. FSD model, case A.

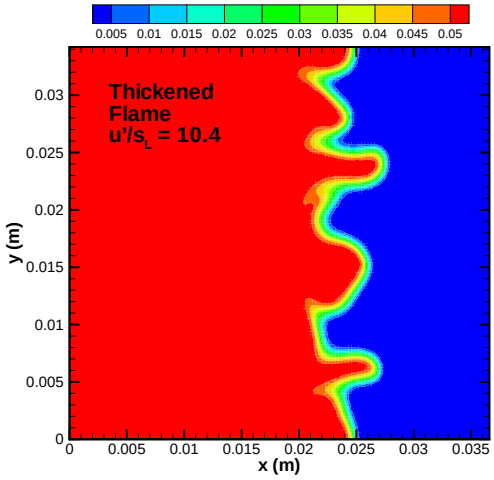

(c) CH_4 mass fraction. Thickened flame, case B, $F = 5$.

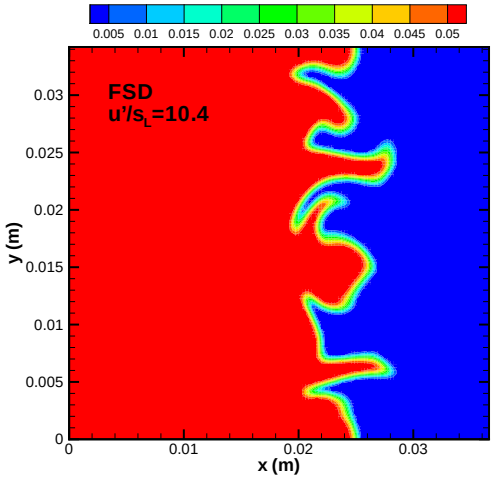

(d) CH_4 mass fraction. FSD model, case B.

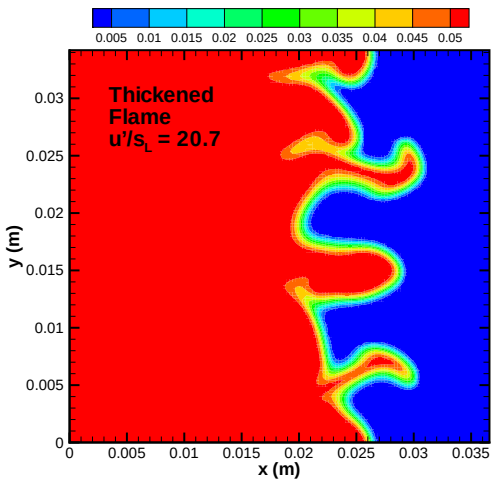

(e) CH_4 mass fraction. Thickened flame, case C, $F = 5$.

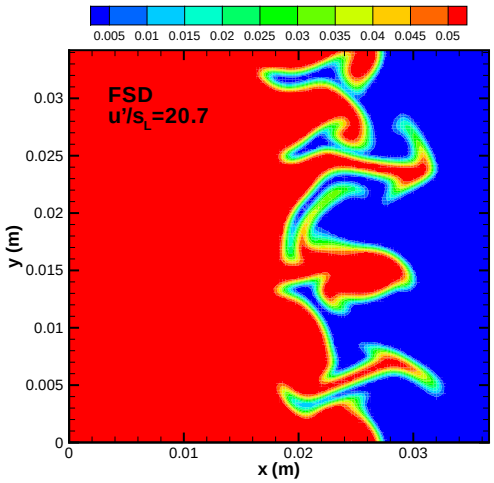

(f) CH_4 mass fraction. FSD model, case C.

Figure 3. Predicted CH_4 contours at 0.6 ms.

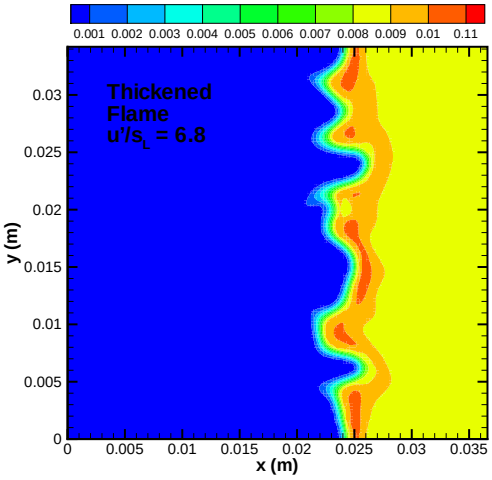

(a) CO mass fraction. Thickened flame, case A, $F = 5$.

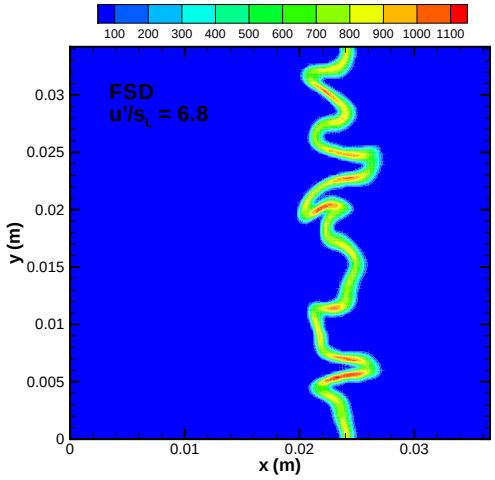

(b) FSD contours. FSD model, case A.

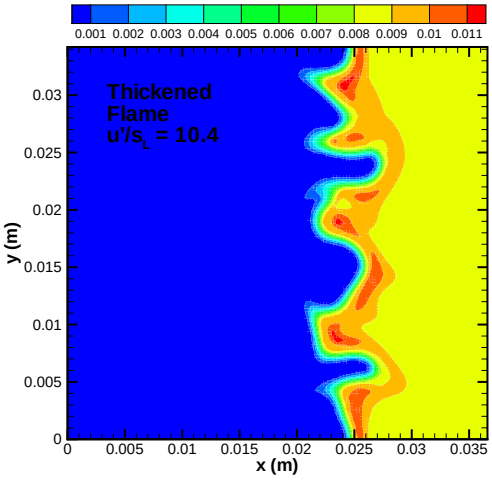

(c) CO mass fraction. Thickened flame, case B, $F = 5$.

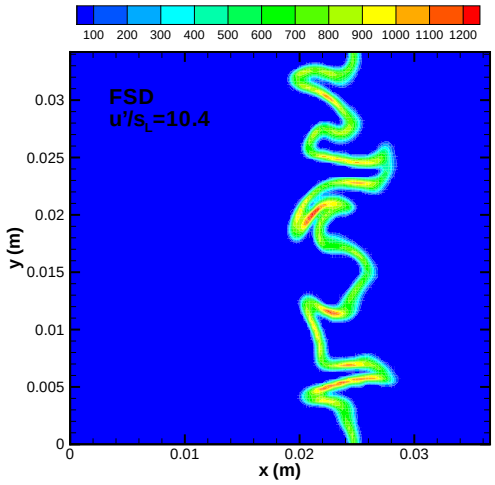

(d) FSD contours. FSD model, case B.

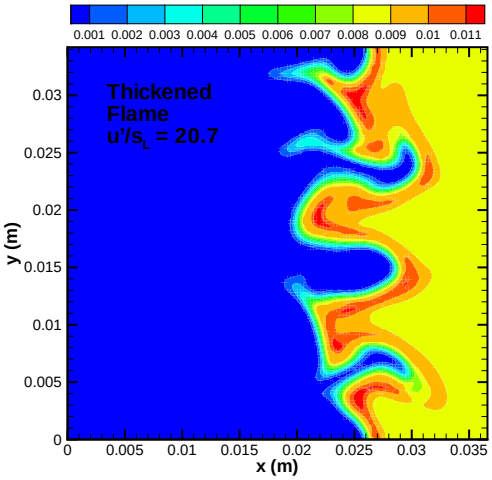

(e) CO mass fraction. Thickened flame, case C, $F = 5$.

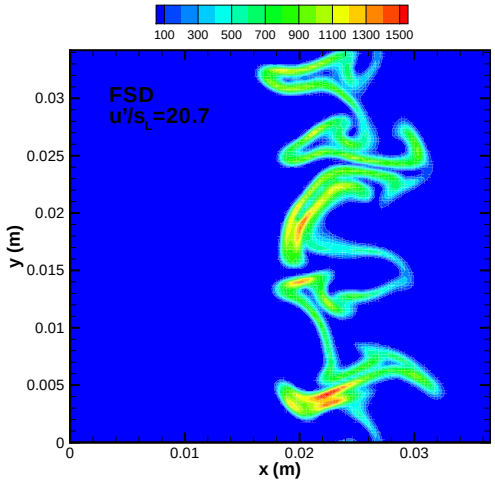

(f) FSD contours. FSD model, case C.

Figure 4. Predicted CO and FSD contours at 0.6 ms.

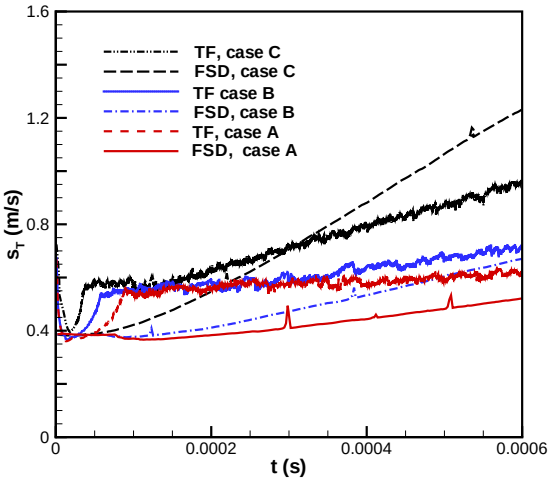

Figure 5. Predicted turbulent burning rates for freely propagating flame in two-dimensional decaying isotropic turbulent fields for Cases A-C.

VI.C. Predicted Turbulent Burning Rates

The predicted turbulent burning rates obtained for both the thickened flame and FSD models for cases A-C are shown in Figure 5. From the figure, it can be seen that there is a short period of adjustment to the initial conditions until the burning rates attain the laminar flame speed. After this initial period of adjustment, the burning rates increase while the flame front is wrinkled by the turbulent flow field. The fuel consumption rate is enhanced by turbulence as more flame surface is produced by the wrinkling of the flame front.

For both models, the computed burning rates follow the same trend, as the turbulence level is increased, more wrinkling is generated with a corresponding increase in the turbulent burning rates. The predicted turbulent flame speeds are quantitatively similar for low turbulence intensities, however, for high turbulence intensity the FSD model predicts a higher flame speed.

VII. Results for Three-Dimensional Freely Propagating Flames

LES predictions of freely propagating flames in fully three-dimensional homogeneous isotropic decaying turbulent fields are now considered. As for the two-dimensional simulations previously described, the three-dimensional turbulent flames are initialized by introducing a planar laminar stoichiometric premixed flame onto a computational domain containing the isotropic turbulent field using the procedure developed by Rogallo.[33] Also as in the two-dimensional simulations, turbulence fields of three different turbulence intensities were considered. These cases are identified as case D, case E, and case F, respectively, and the parameters characterizing the initial turbulent field in the unburnt mixture for each of the cases are as follows: relative turbulence intensity, $u'/s_L = 6.8$ (case D), 10.4 (case E), 20.7 (case F); integral length scale, $L_{11} = 6.5$ mm (case D), 9.9 mm (case E), 19.8 mm (case F); Taylor micro scale, $\lambda = 0.47$ mm (case D), 0.58 mm (case E), 0.82 mm (case F); Komogorov scale, $\eta = 0.046$ mm (case D), 0.037 mm (case E), 0.026 mm (case F); turbulent Reynolds number, $Re_\lambda = 77.19$ (case D), 146.57 (case E), 410.2 (case F); laminar flame speed $s_\mathrm{L} = 0.38$ m/s; and flame thickness, $\delta_\mathrm{L} = 0.44$ mm. A cube-shaped physical domain was considered for the simulation with dimensions of 0.0366 m $\times$ 0.0366 m $\times$ 0.0366 m. Numerical results were obtained using a uniform mesh and the computational domain was discretized using a $108 \times 108 \times 108 = 1,259,712$ cell mesh with the cells equally distributed on 216, 18×18×18-cell, solution blocks. The corresponds to a mesh spacing corresponds of $\Delta x = 0.34$ mm. A filter width of $\Delta = 2\Delta x = 0.68$ mm $= 1.55\delta_\mathrm{L}$ was used when performing the LES. The computational mesh and initial turbulence velocity field for case E are shown in Figures 6(a) and 6(b).

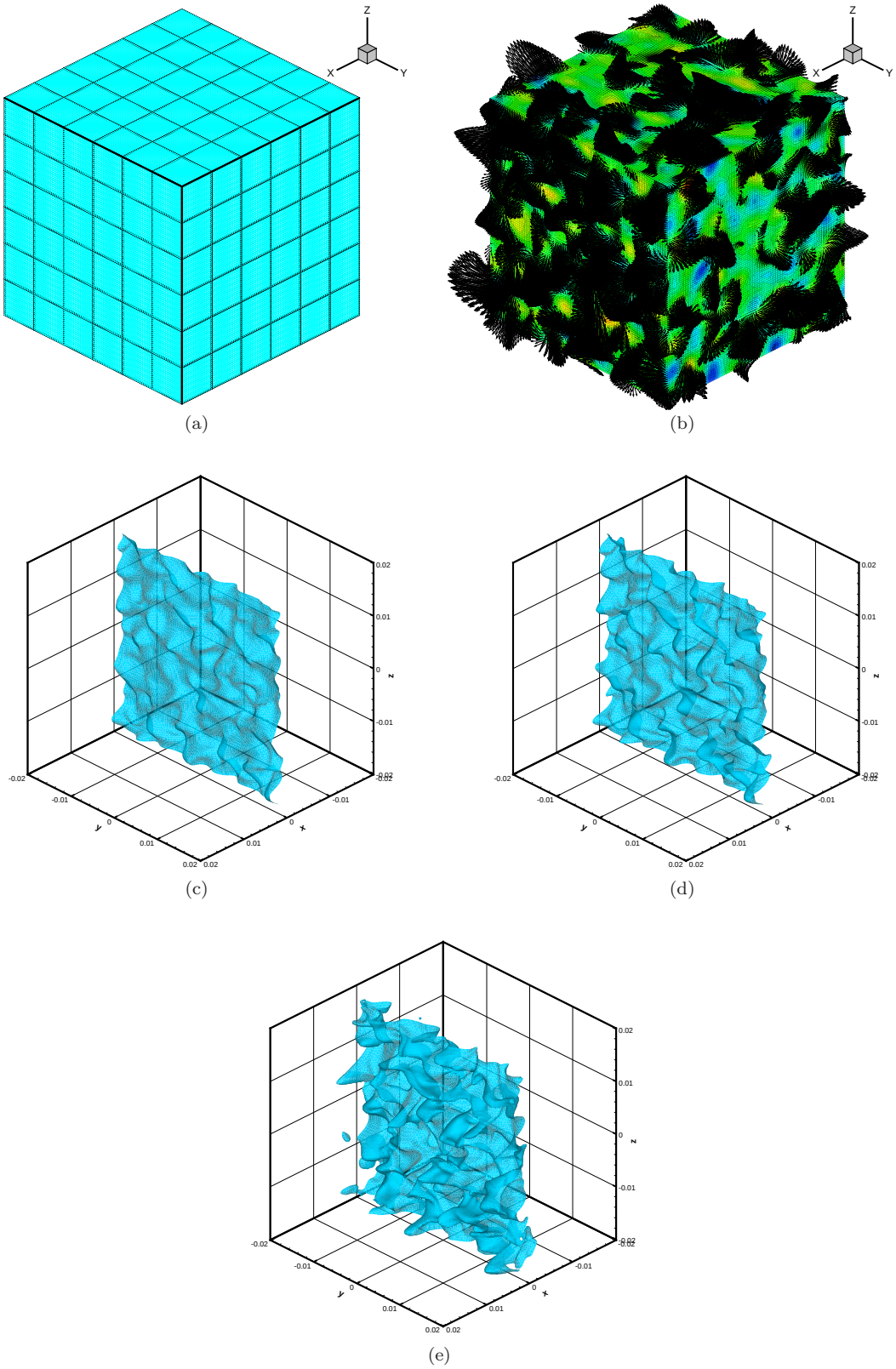

Figure 6. (a) Computational mesh ($108\times108\times108=1,259,712$ cells) and (b) initial turbulent flow field. Predicted iso-surfaces of the progress variable corresponding to $c=0.5$ at time $t=0.3$ ms obtained using the FSD model for turbulence intensities: (c) $u'/s_{\mathrm{L}}=6.8$ (case D); (d) $u'/s_{\mathrm{L}}=10.4$ (case E); and (e) $u'/s_{\mathrm{L}}=20.7$ (case F).

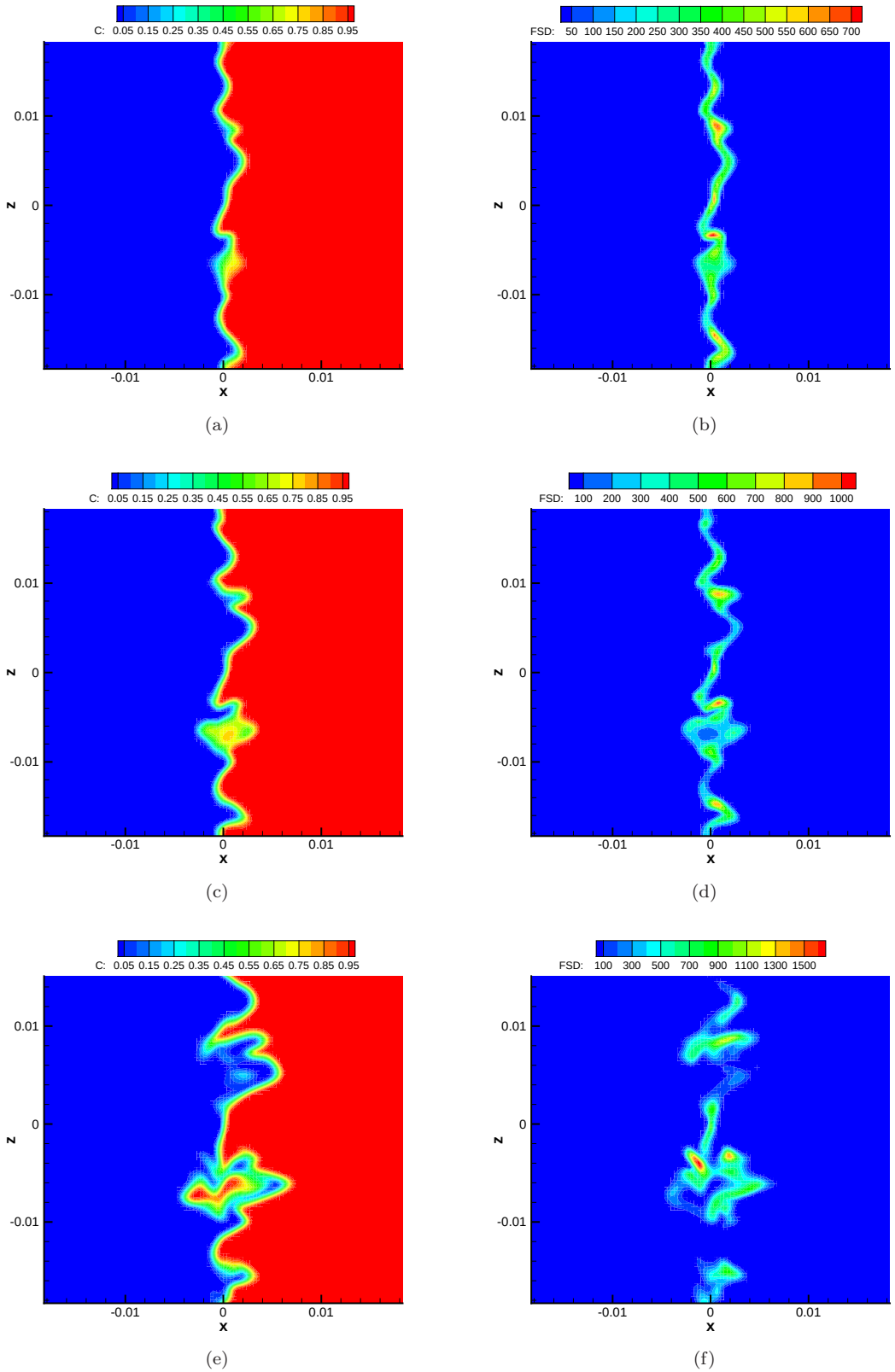

Figure 7. Predicted contours of the progress variable, c, and flame surface density, $\bar{\rho}\tilde{\Sigma}$, for the $y=0$ plane at time $t=0.3$ ms obtained using the FSD model for turbulence intensities: (a) and (b) $u'/s_{\mathrm{L}}=6.8$ (case D); (c) and (d) $u'/s_{\mathrm{L}}=10.4$ (case E); and (e) and (f) $u'/s_{\mathrm{L}}=20.7$ (case F).

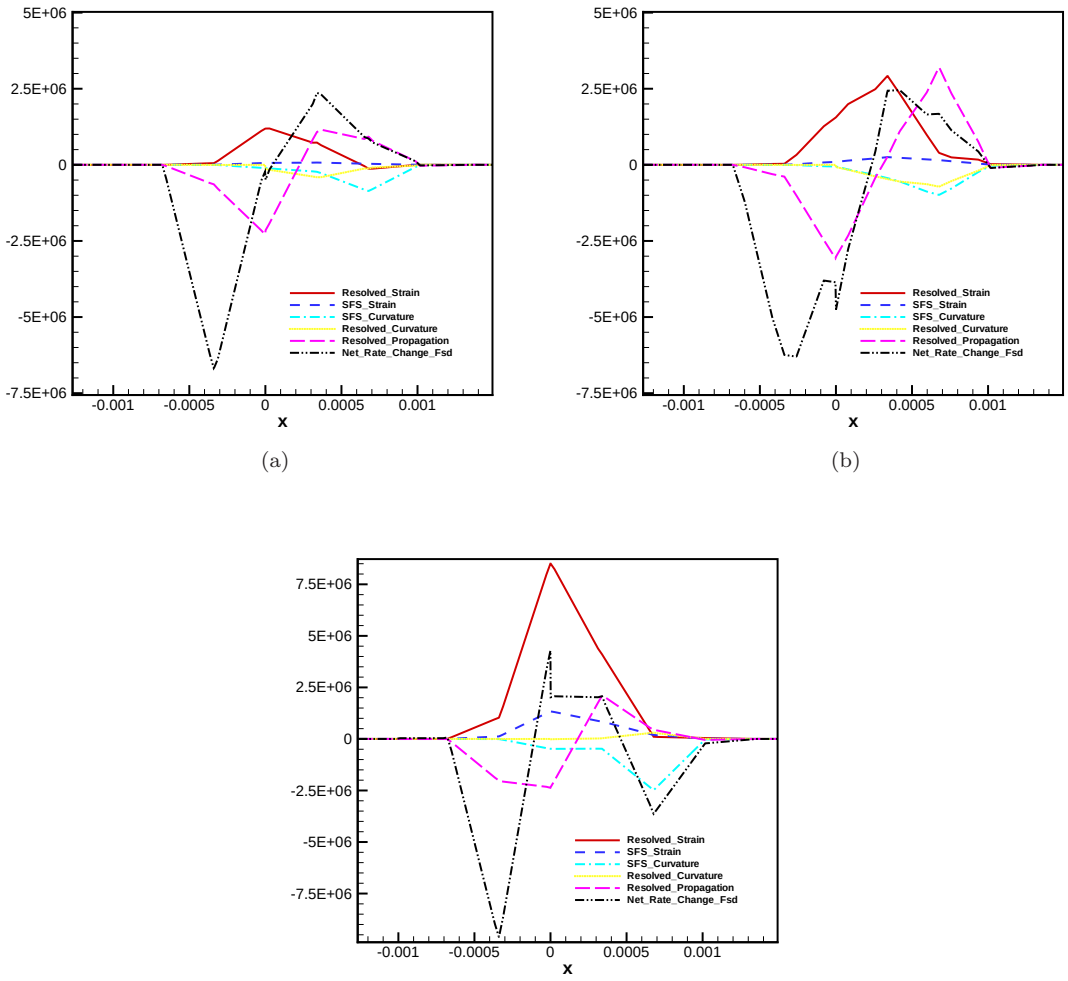

Figure 8. Predicted budget of the production and destruction terms appearing in the transport equation for $\bar{\rho}\tilde{\Sigma}$, . Results are shown for time $t = 0.3$ ms for turbulence intensities: (a) $u'/s_{\rm L} = 6.8$ (case D); (b) $u'/s_{\rm L} = 10.4$ (case E); and (c) $u'/s_{\rm L} = 20.7$ (case F).

Turbulent burning rates for the fully three-dimensional cases are computed as follows:

$$s_{\rm T} = \frac{1}{\bar{\rho}_r \tilde{Y}_{F_r} L_y L_z} \int_V \overline{\dot{\omega}}_F dV \,, \tag{17}$$

and

$$s_{\rm T} = \frac{s_{\rm L}}{L_y L_z} \int_V \bar{\rho}\tilde{\Sigma} dV \,. \tag{18}$$

for the thickened flame and FSD models, respectively.

VII.A. Predicted Flame Structure

Numerical predictions of freely propagating flames for cases D, E, and F, obtained using the FSD model are depicted in Figures 6 and 7. The three-dimensional LES results are shown for the three cases at a time equal to 0.3 ms after initialization. This time corresponds to approximately one and a half, two and three eddy turnovers based on the Taylor scale for each of the cases, respectively. Iso-surfaces of the progress variable corresponding to $c = 0.5$ are shown in Figures 6(c), 6(d), and 6(e) and contour plots of the progress variable,

c, and flame surface density, $\bar{\rho}\tilde{\Sigma}$, for the $y = 0$ plane are given in Figures 7(a)–7(f). The wrinkling of the initially planar flame front is clearly illustrated in Figures 6(c), 6(d), and 6(e). Furthermore, the flame front wrinkling is noticeably increased with increasing turbulence intensity. Although not shown, the increased wrinkling of the flame front also results in a corresponding increase in the predicted burning rate and hence flame propagation speed. The wrinkled structure of the premixed flame fronts are further illustrated in the contour plots of Figures 7(a)–7(f). Although somewhat similar in nature to the two-dimensional results discussed earlier, the predicted flame structures here clearly have a three-dimensional nature.

The ability of LES FSD approach to provide insight into the flame structure is highlighted by the production and destruction terms that appear in the FSD transport equation. The predicted budgets of these production and destruction terms for cases D, E, and F at $t = 0.3$ ms are shown in Figure 8. Referring to the figure, it may be seen that, although somewhat under-resolved on the computational mesh used in the simulations here, there is a complex balance of terms through the flame brush resulting in the final net rate of change of the flame surface density. At the leading edge the main contributions arise from the resolved strain and resolved propagation terms. The largest contributions at the tailing edge of the flame come from the subfilter curvature and resolved propagation terms. As should be expected, the resolved strain term increases significantly with increasing turbulence intensity. It is evident there are strong spatial variations in the resolved source terms that would simply not be observable in or predicted by a Reynolds- or Favre-averaged Navier-Stokes simulation of the premixed flame.

VIII. Concluding Remarks

Numerical results for two- and three-dimensional turbulent premixed flames have been described and comparisons were made between the predicted flame structure and turbulent burning rates as a function of turbulence intensity. Two subfilter scale models were employed, one based on the thickened flame model and the other based on a modeled transport equation for the flame surface density. All in all, there is qualitative agreement between the two models and the same trends were observed on the numerical solutions. Both approaches offer advantages and disadvantages from both physical and computational points of view. Future research will involve more detailed comparisons of the predictive capabilities of the two subfilter scale models for more practical premixed flame configurations.

Acknowledgments

This research has been funded by a Natural Sciences and Engineering Research Council of Canada Collaborative Research Opportunity (NSERC-CRO) grant. The second author also gratefully acknowledges the financial support provided by the Mexican National Council for Science and Technology.

References

[1]Piomelli, U., "Large-Eddy Simulation: Achievements and Challenges," *Prog. Aerospace Sci.*, Vol. 35, 1999, pp. 335–362.

[2]Pitsch, H., "Large-Eddy Simulation of Turbulent Combustion," *Ann. Rev. Fluid Mech.*, Vol. 38, 2006, pp. 453–482.

[3]Colin, O., Ducros, F., Veynante, D., and Poinsot, T., "A Thickened Flame Model for Large Eddy Simulations of Turbulent Premixed Combustion," *Phys. Fluids*, Vol. 12, 2000, pp. 1843–1863.

[4]Charlette, F., Meneveau, C., and Veynante, D., "A power-law flame wrinkling model for LES of premixed turbulent combustion, part I: non-dynamic formulation and initial tests," *Combust. Flame*, Vol. 131, 2002, pp. 159–180.

[5]Hawkes, E. R., *Large Eddy Simulation of Premixed Turbulent Combustion*, Ph.D. thesis, University of Cambridge, July 2000.

[6]Hawkes, E. R. and Cant, R. S., "Implications of a Flame Surface Density Approach to Large Eddy Simulation of Premixed Turbulent Combustion," *Combust. Flame*, Vol. 126, 2001, pp. 1617–1629.

[7]Peters, N., *Turbulent Combustion*, Cambridge University Press, Cambridge, 2000.

[8]Northrup, S. A. and Groth, C. P. T., "Solution of Laminar Diffusion Flames Using a Parallel Adaptive Mesh Refinement Algorithm," Paper 2005–0547, AIAA, January 2005.

[9]Gao, X. and Groth, C. P. T., "Parallel Adaptive Mesh Refinement Scheme for Turbulent Non-Premixed Combusting Flow Prediction," Paper 2006-1448, AIAA, January 2006.

[10]Veynante, D. and Vervisch, L., "Turbulent Combustion Modeling," *Progress in Energy and Combustion Science*, Vol. 28, 2002, pp. 193–266.

[11]Smagorinski, J., "General Circulation Experiments with te Primitive Equations. I: The Basic Experiment," *Monthly Weather Review*, Vol. 91, No. 3, 1979, pp. 99–165.

[12]Yoshizawa, A., "Statistical theory for compressible turbulent shear flows, with the application to subgrid modeling," *Phys. Fluids A*, Vol. 29, 1986, pp. 2152–2164.
[13]Knight, D., Zhou, G., Okong'o, N., and Shukla, V., Paper 98-0535, AIAA, January 1998.
[14]O'Rourke, P. J. and Bracco, F. V., "Two Scaling Transformations for the Numerical Computation of Multidimensional Unsteady Laminar Flames," *J. Comput. Phys.*, Vol. 33, 1979, pp. 185–203.
[15]Charlette, F., Meneveau, C., and Veynante, D., "A power-law flame wrinkling model for LES of premixed turbulent combustion, part II: dynamic formulation," *Combust. Flame*, Vol. 131, 2002, pp. 181–197.
[16]Meneveau, C. and Poinsot, T., "Stretching and quenching of flamelets in premixed turbulent combustion," *Combust. Flame*, Vol. 86, 1991, pp. 311–332.
[17]Gao, X. and Groth, C. P. T., "Parallel Adaptive Mesh Refinement Scheme for Three-Dimensional Turbulent Non-Premixed Combustion," Paper 2008-1017, AIAA, January 2008.
[18]Barth, T. J., "Recent Developments in High Order K-Exact Reconstruction on Unstructured Meshes," Paper 93-0668, AIAA, January 1993.
[19]Roe, P. L., "Approximate Riemann Solvers, Parameter Vectors, and Difference Schemes," *J. Comput. Phys.*, Vol. 43, 1981, pp. 357–372.
[20]Liou, M.-S., "A Sequel to AUSM, Part II: AUSM$^+$-up for all Apeeds," *J. Comput. Phys.*, Vol. 214, 2006, pp. 137–170.
[21]Coirier, W. J. and Powell, K. G., "An Accuracy Assessment of Cartesian-Mesh Approaches for the Euler Equations," *J. Comput. Phys.*, Vol. 117, 1995, pp. 121–131.
[22]Weiss, J. M. and Smith, W. A., "Preconditioning Applied to Variable and Constant Density Flows," *AIAA J.*, Vol. 33, No. 11, 1995, pp. 2050–2057.
[23]Gropp, W., Lusk, E., and Skjellum, A., *Using MPI*, MIT Press, Cambridge, Massachussets, 1999.
[24]Sachdev, J. S., Groth, C. P. T., and Gottlieb, J. J., "A Parallel Solution-Adaptive Scheme for Predicting Multi-Phase Core Flows in Solid Propellant Rocket Motors," *Int. J. Comput. Fluid Dyn.*, Vol. 19, No. 2, 2005, pp. 157–175.
[25]Gordon, S. and McBride, B. J., "Computer Program for Calculation of Complex Chemical Equilibrium Compositions and Applications I. Analysis," Reference Publication 1311, NASA, 1994.
[26]McBride, B. J. and Gordon, S., "Computer Program for Calculation of Complex Chemical Equilibrium Compositions and Applications II. Users Manual and Program Description," Reference Publication 1311, NASA, 1996.
[27]Wilke, C. R., "A Viscosity Equation for Gas Mixtures," *J. Chem. Phys.*, Vol. 18, 1950, pp. 517–519.
[28]Gardiner, W. C., *Combustion Chemistry*, Springer-Verlag New York Inc., Boca Raton, 1984.
[29]Westbrook, C. K. and Dryer, F. L., "Simplified Reaction Mechanisms for the Oxidation of Hydrocarbon Fuels in Flames," *Combust. Sci. Tech.*, Vol. 27, 1981, pp. 31–43.
[30]Cant, R. S., Rutland, C. J., and Trouvé, A., "Statistics for laminar modeling," *Proceedings of the Summer Program*, Center for Turbulence Research, 1990, pp. 271–279.
[31]Girimaji, S. S. and Pope, S. B., "Propagating surfaces in isotropic turbulence," *J. Fluid Mech.*, Vol. 234, 1992, pp. 247–277.
[32]Haworth, D. C. and Poinsot, T. J., "Numerical Simulations of Lewis Number Effects in Turbulent Premixed Flames," *J. Fluid Mech.*, Vol. 244, 1992, pp. 405–436.
[33]Rogallo, R. S., "Numerical Experiments in Homogeneous Turbulence," NASA Technical Memorandum 81315, 1981.
[34]Hawkes, E. R. and Chen, J. H., "Direct numerical simulation of hydrogen-enriched lean premixed methane-air flames," *Combust. Flame*, Vol. 138, 2004, pp. 405–436.
[35]Echekki, T. and Chen, J. H., "Unsteady strain rate and curvature effects in turbulent premixed methane-air flames," *J. Comput. Phys.*, Vol. 118, 1996, pp. 24–37.